Nucleic Acids Research, 2025, **53**, gkaf884
https://doi.org/10.1093/nar/gkaf884
RNA and RNA-protein complexes

Ligand specificity and adaptability revealed by the first Guanine-II riboswitch tertiary structure

Hongcheng Li†, Xin Shen†, Xiaochen Xu, Xiaoqing Tai, Mengqi He, Jinzhu Zhang*, Aiming Ren*

Department of Cardiology of The Second Affiliated Hospital and Life Sciences Institute and School of Medicine, Zhejiang University, Hangzhou 310058, China

*To whom correspondence should be addressed. Email: aimingren@zju.edu.cn
Correspondence may also be addressed to Jinzhu Zhang. Email: jinzhuzhang@zju.edu.cn
†The first two authors should be regarded as Joint First Authors.

Abstract

A comprehensive understanding of the fundamental principles governing RNA–small molecule interactions is crucial for advancing RNA-targeting therapeutics with small molecules. Riboswitches, a class of noncoding RNAs, regulate gene expression by direct interaction with small-molecule metabolites. In this work, we report an in-depth structure-based investigation of a newly identified riboswitch, Guanine-II, which, despite sharing a conserved scaffold with the Guanine-I riboswitch, exhibits strikingly distinct small molecule ligand-binding characteristics. Through a comprehensive structural analysis of the Guanine-II riboswitch bound to various guanine analogs, combined with comparative studies of other guanine riboswitch variants, including Guanine-I and Xanthine-II riboswitches, as well as isothermal titration calorimetry, we reveal local structural rearrangements that precisely modulate small-molecule ligand adaptability. We further demonstrate that subtle differences in the composition and peripheral architecture of the binding pocket are key determinants of ligand-binding specificity. Additionally, based on the similarity in ligand recognition patterns with the tetrahydrofolate-II riboswitch, we identified additional compounds that bind to the Guanine-II riboswitch through a structure-guided rational search, providing valuable structural insights for the discovery of small molecules targeting RNA.

Graphical abstract

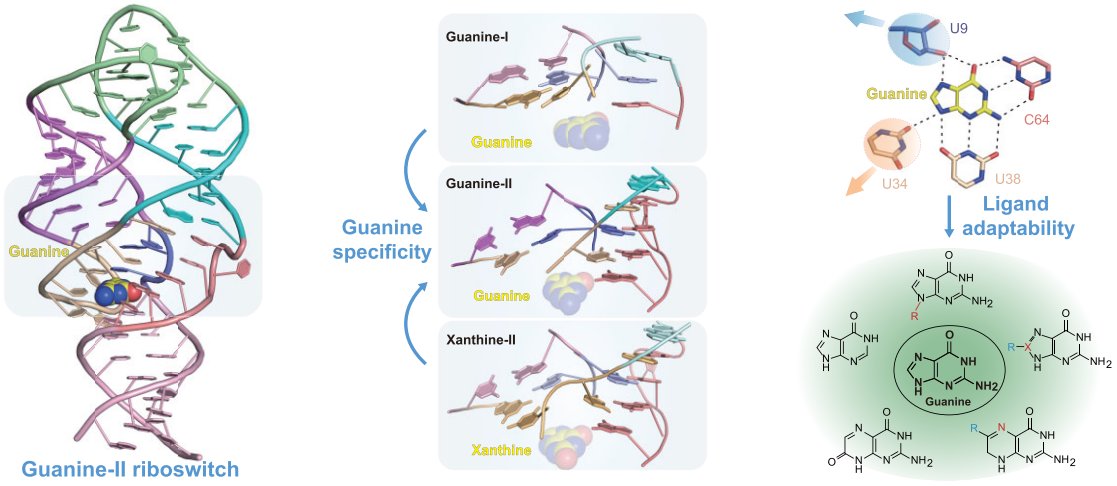

Introduction

Riboswitches are conserved genetic elements located in the 5′-UTR regions of messenger RNA, consisting of a specific ligand-binding domain and a flexible expression platform [1–5]. The ligand-binding domain selectively recognizes specific small-molecule metabolites, and the subsequent ligand-induced structural change triggers an "ON or OFF" switch in the expression platform, thereby regulating the downstream gene expression processes such as transcription, translation, or alternative splicing [6]. Most riboswitches regulate genes involved in the biosynthesis and transport of their ligands, establishing riboswitches as a critical feedback mechanism for maintaining the homeostasis of biological metabolite concentrations.

Since the identification of the first riboswitches two decades ago, at least 55 distinct types of riboswitches have been iden-

Received: June 6, 2025. **Revised:** August 13, 2025. **Editorial Decision:** August 15, 2025. **Accepted:** August 21, 2025

tified [6–8]. Riboswitches are widely distributed across bacteria, archaea, and plants [9]. Depending on their bound ligands, riboswitches are broadly classified into six major families, including these that bind purines and derivatives, enzyme cofactors and derivatives, amino acids, metals, anions, and others [6]. Among these, purine- and purine-derivative-binding riboswitches represent one of the most abundant classes across all known riboswitches [6, 10]. These riboswitches play critical roles in cellular functions, as purines are not only fundamental components of genetic material but also act as key cellular signaling molecules (e.g. ATP, cAMP, and cGMP) and cofactors (e.g. NAD^+, FAD, and Coenzyme A). Additionally, purine molecules are essential to energy metabolism, with ATP and GTP serving as primary energy carriers in the cell (e.g. ATP and GTP) [11, 12]. The versatility and regulatory capacity of purine-responsive riboswitches underscore their importance in maintaining cellular homeostasis and adapting to metabolic demands.

In 2003, the Guanine-I riboswitch was identified as one of the earliest classes of metabolite-responsive riboswitches [13]. This riboswitch is widely distributed in both Gram-positive and Gram-negative bacteria and is typically associated with genes involved in purine biosynthesis, recycling, or uptake. Structural analysis of the Guanine-I riboswitch has revealed a highly conserved secondary structure characterized by a three-way junction (Supplementary Fig. S1), where guanine is specifically recognized through conserved bases. Notably, the Guanine-I riboswitch also exhibits binding affinity for several purine derivatives, including hypoxanthine, xanthine, guanosine, and 2′-deoxyguanosine (2′-dG) [13, 14]. High-resolution crystal structures of Guanine-I riboswitch–ligand complexes have provided critical insights into its molecular recognition mechanism [15–17]. These studies highlighted how specific base-pairing interactions, hydrogen bonding, and stacking interactions shape the tertiary structural fold of Guanine-I riboswitch and contribute to the high specificity and selectivity of guanine recognition. The structural plasticity of the Guanine-I riboswitch allows it to accommodate structurally similar metabolites, while maintaining its regulatory function.

In 2022, a novel variant of the guanine riboswitch, designated as Guanine-II, was discovered in several bacterial species, including *Paenibacillus*, *Propionispira*, and an unnamed *Clostridium* species [18]. In comparison to the well-characterized Guanine-I riboswitch, the Guanine-II variant features distinct nucleotide changes, notably the insertion of a base at J2/3 junction and three or four bases at J3/1 junction (Supplementary Fig. S1). Compared to the Guanine-I riboswitch, the Guanine-II riboswitch exhibits altered ligand specificity, showing no binding affinity for xanthine and reduced affinity for hypoxanthine [18]. Functional analysis and studies in *Paenibacillus* bacteria revealed that these two riboswitches regulate distinct sets of downstream genes and exert opposing regulatory effects [13, 18]. Specifically, upon binding to guanine, the Guanine-I riboswitch represses the expression of downstream genes associated with the xanthine phosphoribosyltransferase (XPRTase) [13]. In contrast, the Guanine-II riboswitch activates the expression of genes encoding enzymes of the phosphoribosyltransferase-I (PRT-I) family in response to guanine binding [18].

To elucidate the tertiary folding pattern and the ligand recognition mechanism of the Guanine-II riboswitch, we determined the crystal structures of the PRT (phosphoribosyltransferase) riboswitch in complex with guanine, hypoxanthine, guanosine, and 2′-dG. These high-resolution structures revealed key structural elements governing ligand selectivity and binding affinity. Subsequently, we employed isothermal titration calorimetry (ITC) to quantitatively determine the binding affinities of structure-based mutants of the Guanine-II riboswitch for guanine, as well as the affinity of the wild-type (WT) Guanine-II riboswitch for various ligands. To further refine our understanding of the Guanine-II riboswitch, we conducted a comparative structural analysis with Guanine-I and Xanthine-II riboswitches, focusing on overall architecture, binding pocket composition, and ligand specificity. This comparison revealed distinct structural features in the junctional regions and ligand-binding pockets that modulate specificity for guanine and its derivatives. Notably, we identified a single-nucleotide switching mechanism in the binding site that dictates ligand preference, underscoring the evolutionary divergence between these riboswitch classes. In addition, inspired by the similar ligand recognition pattern observed between Guanine-II and Tetrahydrofolate-II (THF-II) riboswitches, we also searched for additional compounds capable of binding to the Guanine-II riboswitches, validated the binding of these compounds using ITC, and explored the molecular basis underlying the binding by determination of their co-crystal structures with the riboswitch, not only highlighting the conserved recognition strategies employed by structurally distinct RNA folds, but also provides a platform to expand the scope of riboswitch-binding compounds, laying a structural foundation for the discovery of small molecules targeting riboswitches and the rational design of potential antimicrobial agents.

Materials and methods

RNA preparation for crystallization

Based on the conserved sequence of the Guanine-II riboswitch, we designed various base pairs for the P1 stem and added an additional G nucleotide at the 5′ end. The sequences of Guanine-II riboswitch and hammerhead self-cleavage ribozyme were inserted into the pUT7 plasmid [19], and the DNA template for *in vitro* transcription was obtained by polymerase chain reaction (PCR). Subsequently, *in vitro* transcription was performed to produce full-length RNA using T7 RNA polymerase at 37°C for 4.5 h. The detailed protocol of transcription of RNA and cleavage of ribozyme can be found in the previous article [19]. The target RNA and ribozyme RNA were separated by urea-denatured polyacrylamide gel electrophoresis. The gel fragment containing the target RNA was excised under 254 nm UV illumination and soaked in 0.5× Tris–acetate–EDTA buffer. The leaching solution was sequentially precipitated with isopropanol and ethanol, and washed twice with 80% ethanol. After lyophilization, the RNA was dissolved in diethylpyrocarbonate (DEPC)-treated water.

Ligand

Guanine, hypoxanthine, guanosine, 2′-deoxyguanosine, 8-aminoguanine, 8-azaguanine, pterin, isoxanthopterin, 7,8-dihydroneopterin, and tetrahydrobiopterin were purchased from Yuanye Bio-Technology Co. Ltd (Shanghai).

Crystallization

RNA samples of the Guanine-II riboswitch were diluted to a final concentration of 0.4 mM in a buffer containing 40 mM HEPES (pH 7.4), 50 mM KCl, and 5 mM $MgCl_2$, followed by annealing at 65°C for 5 min and incubated on ice for 30 min. The ligand was then added with a final concentration of 5 mM and the mixture was kept on ice for an additional 30 min. Precipitates were removed by centrifugation at 12 000 × *g* and 4°C. Crystallization experiments were performed using the sitting drop vapor diffusion method by mixing 0.18 μl RNA solution and reservoir solution in a 1:1 volume ratio. About a week later, well-diffracting crystals of the construct bound to guanine or other ligands grew in the buffer containing 0.08 M sodium chloride, 0.04 M sodium cacodylate trihydrate (pH 7.0), 30% (v/v) (±)-2-methyl-2,4-pentanediol, and 0.012 M spermine tetrahydrochloride. The crystals exhibit a tabular shape with a rectangular morphology, measuring ∼0.05–0.1 mm in size. Then, the crystals were frozen directly from drops with liquid nitrogen and transported to the Shanghai Synchrotron Radiation Facility (SSRF) for X-ray diffraction data collection. X-ray diffraction data for the guanine-bound Guanine-II complex were collected at the BL19U1 beamline, using a wavelength of 1.10202 Å (Supplementary Table S1). The crystal-to-detector distance was set to 300 mm, and 360 diffraction images were collected with a 1° oscillation angle ($\Delta\varphi$) per image. A DECTRIS PILATUS 6M Detector was used, and each dataset was collected from a single crystal.

Structure determination and refinement

The crystal diffraction data were processed using HKL3000 (HKL Research). The molecular replacement (MR) in the Phenix software suite was performed to solve the phase problem and the refinement procedures in Phenix and Coot were used to build and complete the crystal structure model [20–22]. After the RNA model was built, the ligand was incorporated into the structure based on the electron density map. All statistical results of X-ray diffraction data collection and structure refinement are listed in Supplementary Table S1.

Isothermal titration calorimetric experiment

All ITC experiments were performed using the ITC200 Microcalorimeter at the National Center for Protein Science Shanghai (NCPSS). Prior to the experiments, all RNA and ligand titration samples were dialyzed in the ITC buffer containing 40 mM HEPES (pH 7.4), 50 mM KCl, and 10 mM $MgCl_2$ at 4°C. To determine the influence of Mg^{2+} on the binding of RNA and guanine, the concentration of $MgCl_2$ in the ITC buffer was varied from 0 to 20 mM. RNA titration samples were diluted to a final concentration of 0.05–0.5 mM, annealed at 65°C for 5 min, and incubated on ice for 30 min. 0.18 or 0.5 mM RNA were titrated into the sample cell containing 200 μl of 0.018 mM guanine or 0.05 mM xanthine by initial injection of 0.4 μl, followed by 18 serial injections of 2 μl, with the interval of 120 s and a reference power of 5 μcal s^{-1}. 0.5–1 mM other ligands were titrated into the sample cell containing 200 μl of 0.05 mM RNA. 0.5 mM RNA was titrated into the sample cell containing the ITC buffer as the background heat, which was subtracted when calculating the parameters of RNA bound to xanthine. Each experiment was performed in duplicate or higher numbers of replicates. All the binding constants and thermodynamic values are listed in Supplementary Table S2.

EGFP reporter assays

The WT and mutants of the Guanine-II riboswitch were amplified by PCR and cloned into the vector pUCm-T upstream of the enhanced greenfluorescent protein (EGFP) gene. The plasmids were transformed into DH5α, and a single colony was inoculated into 3 ml of LB medium and cultured for 8 h. The bacterial culture was diluted ∼10-fold to achieve the same OD_{600}. This step normalized the bacterial cell numbers across samples to ensure equal starting cell density and then incubated for 48 h at 37°C with shaking at 220 rpm. Due to the presence of abundant endogenous ligands capable of binding the Guanine-II riboswitch, a strain completely lacking all endogenous ligand biosynthesis pathways could not be used for the EGFP experiment, and thus the influence of endogenous ligands was not excluded. No exogenous ligands were added in this experiment; activation of the riboswitch was solely mediated by endogenous ligands. The fluorescence of all reporter assay samples was measured using a Synergy Neo2 MultiMode Microplate Reader (BioTek) with excitation at 488 nm and emission at 550 nm. The EGFP expression assay was performed in three biological replicates. Background fluorescence was subtracted using strains lacking EGFP expression.

Results and discussion

Crystallization and tertiary structure of the PRT riboswitch in complex with guanine

The secondary structure of the Guanine-II riboswitch features a large junction (J1/2, J2/3, and J3/1) that connects the stems P1, P2, and P3 (Fig. 1A), conforming to the typical three-stem junction fold of purine riboswitches [7, 14, 18, 23]. Based on the consensus sequences of the Guanine-II riboswitch, we screened a variety of RNA constructs for crystallization in the presence of guanine and successfully obtained high-quality, well-diffracting crystals of one RNA construct (named PRT riboswitch) comprising 71 nucleotides derived from *Paenibacillus sp.* FSL. The first determined structure in our manuscript is the Guanine-II riboswitch bound to guanine, which was solved using MR method, with the Guanine-I riboswitch structure (PDB: 6UBU) as the initial model [24]. All subsequent ligand-bound structures were also determined by MR, using Guanine-II structure as the initial model. All nucleotides were observed in each structure, with only minor nucleotide disorder. In cases where electron density around nucleotide U35 was weak, the ribose moiety still exhibited defined density. The resolution range, R_{work}/R_{free} values, and other relevant structural statistics are provided in Supplementary Table S1, following standard criteria for crystal structure determination [25]. The R_{free}/R_{work} values indicate that none of the structures are overfitted.

The crystal structure resolution of the PRT Guanine-II riboswitch in complex with guanine was determined at a resolution of 2.75 Å (X-ray crystallography statistic data are listed in Supplementary Table S1). To access the binding affinity of PRT RNA with guanine in the presence of 10 mM $MgCl_2$, we performed ITC, which revealed a dissociation constant (K_d) of 0.013 ± 0.002 μM (Fig. 1B, Supplementary Fig. S2A, and Supplementary Table S2). The binding stoichiometry approached 1:1, with guanine binding driven by a favorable enthalpy ($\Delta H = -20.9 \pm 0.1$ kcal mol^{-1}) that offsets an unfavorable entropy component (+10.2 kcal mol^{-1}) giving rise

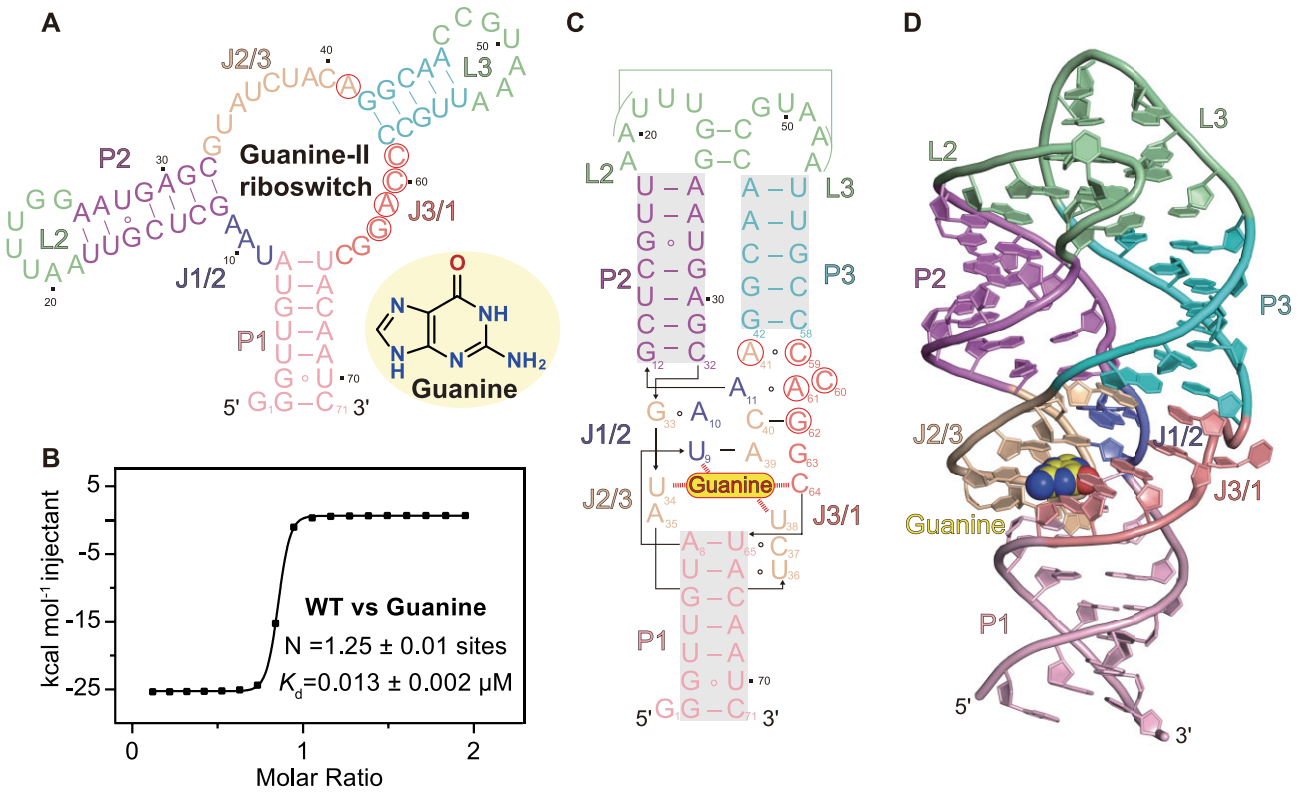

Figure 1. Secondary and tertiary structure of the Guanine-II riboswitch. (**A**) The secondary structure of *Paenibacillus sp.* FSL 92 PRT Guanine-II riboswitch and chemical structure of guanine. The characteristic inserted nucleotides unique to the Guanine-II riboswitch are labeled with red circles. The oxygen atom and nitrogen-containing groups in guanine are highlighted in bold red and bold blue, respectively. (**B**) ITC experiment of the PRT Guanine-II riboswitch binding to guanine. Three replicates are shown in Supplementary Fig. S2. (**C**) Schematic representation of the tertiary structure of the PRT Guanine-II riboswitch, with the featured inserted nucleotides labeled by red circle. The same color code as the cartoon representation in panel (D) is used. (**D**) Cartoon representation of the tertiary structure of the PRT Guanine-II riboswitch bound to guanine (shown in sphere).

to a ΔG of -10.8 kcal mol^{-1} (Fig. 1B and Supplementary Table S2).

The schematic secondary structure and cartoon representation of the tertiary structure of PRT riboswitch are shown in Fig. 1C and D. Consistent with the conserved motif of the secondary structure, the Guanine-II riboswitch forms three stems (P1 in light pink, P2 in violet, and P3 in cyan), connected by the central junction, which is divided into three regions by the stems and termed J1/2 (in slate), J2/3 (in wheat), and J3/1 (in salmon). These elements together create a continuous spiral stacking conformation (Supplementary Fig. S2B). The bound guanine is encapsulated in the binding pocket formed by the three junction regions. Terminal loops L2 and L3 (in pale green) participate in long-distance interactions through two base quartets, U21-G24-C48-A52 and A20-G25-C47-A53 (Supplementary Fig. S3A and B). G24 and G25 from loop L2 form regular Watson–Crick base pairs with C48 and C47 from loop L3, respectively (Supplementary Fig. S3C and D). These parallel stacks of base quartets reinforce the termini of stems P2 and P3 together, stabilizing the upper part conformation (loops L2 and L3) of the overall fold (Fig. 1D). ITC experiments with mutants revealed that substitutions at G24 (G24C) and G25 (G25C), which disrupt the Watson–Crick interactions, significantly reduced the binding affinity of the riboswitch (Supplementary Fig. S3E and Supplementary Table S2). In contrast, mutations at A52 (A52U) and A53 (A53C), which alter noncanonical pairing interactions, did not notably affect the binding affinity (Supplementary Fig. S3E and Supplementary Table S2). The L2 and L3 loops of the Guanine-I and Guanine-II riboswitches are aligned to compare the long-distance interactions, which shows similar conformation from the root mean square deviation (RMSD) value of 0.613 Å (Supplementary Fig. S3F). Guanine-II only has two different nucleotides in L2 (A19 and U22) compared to Guanine-I (G32 and A35). A35 forms a *trans* Watson–Crick/Hoogsteen base pair with A64 in Guanine-I, whereas in Guanine-II, U22 does not interact with A51 (Supplementary Fig. S3F and G). However, both Guanine-I and Guanine-II form two identical base quartets with the same interactions (Supplementary Fig. S3G).

Structural organization of the junctions

The three parts of the PRT riboswitch junction (J1/2, J2/3, and J3/1) collectively twist and fold in a coordinated manner, interacting intricately with each other to form the binding pocket for guanine and stabilize the overall fold of the tertiary structure. A schematic diagram of PRT riboswitch highlighting the three parts of the junction around guanine binding pocket is shown in Fig. 2A, while an expanded view of their tertiary structure is shown in Fig. 2B. In the lower part of the junction, U36 and C37 in J2/3 interact with the sugar edge of A66 and U65, respectively, forming the U7-A66·U36 and A8-U65·C37 base triplets at the terminal of stem P1. These interactions stabilize both the conformation of J2/3 and stem P1 (Supplementary Fig. S4A and B, and Fig. 2B). In the up-

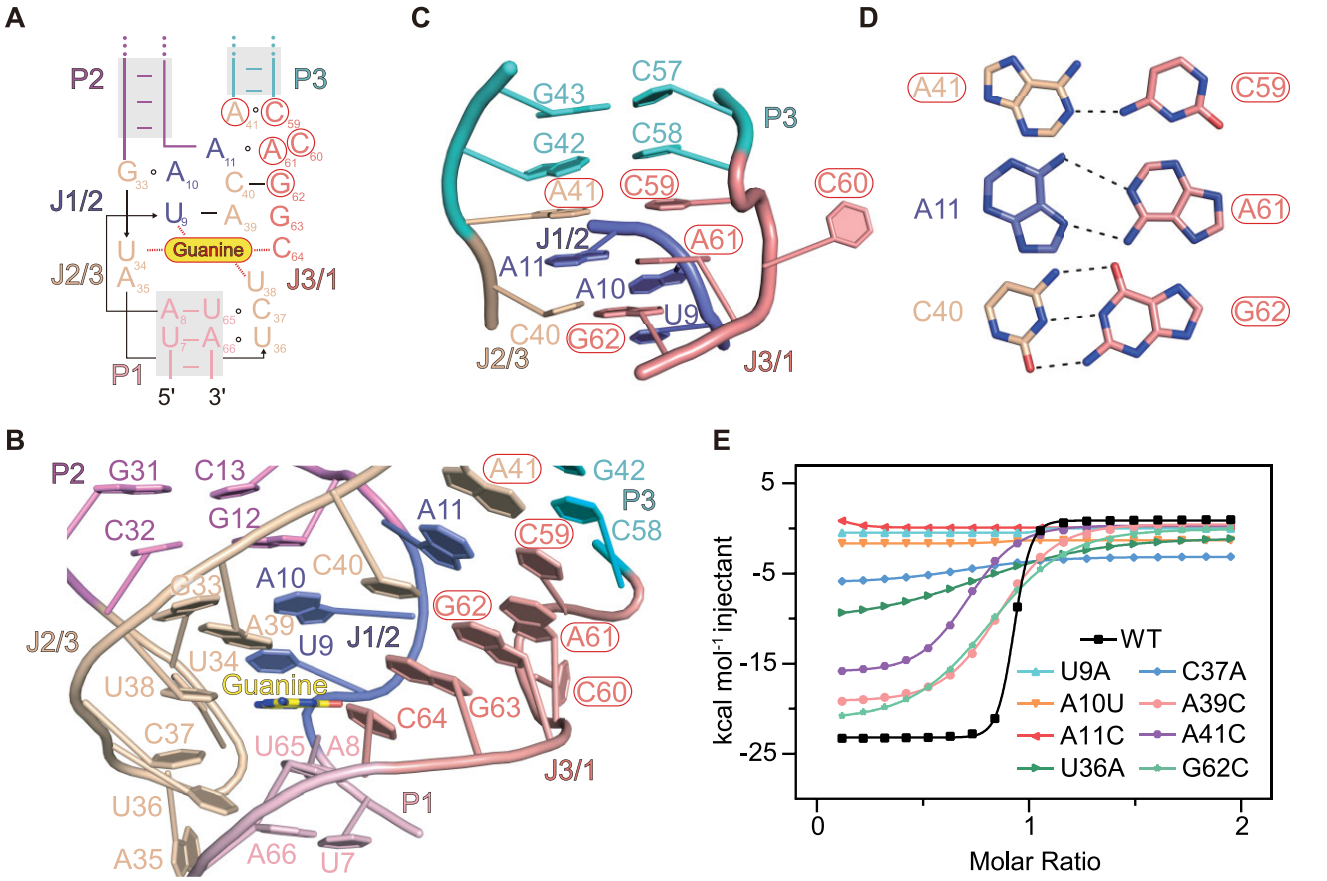

Figure 2. Long-distance interactions in the junction of the PRT Guanine-II riboswitch. (**A**) Schematic secondary structure of the PRT Guanine-II riboswitch with the core region highlighted. Three stems are shaded in gray. The characteristic-inserted nucleotides unique to the Guanine-II riboswitch are labeled with red circles. (**B**) An expanded view of long-distance interactions between the three junction regions. (**C**) An expanded view of stacking interactions between P3 and three junction regions. (**D**) Hydrogen-bonding interactions of the featured inserted nucleotides (A41, C59–G62) in the junction, including A41·C59, A11·A61, and C40·G62. (**E**) Overlay of ITC titration heat plots of Guanine-II riboswitch in comparison with mutants concerning nucleotides in the junctions. WT refers to the wildtype PRT riboswitch in Fig. 1A.

per part of the junction, U9 in J1/2 forms a *cis* Watson–Crick pair with A39 in J2/3, while A10 in J1/2 interacts with G33 in J2/3 through a *cis* Watson–Crick/sugar edge pairing. These interactions further enhance the stability and compactness of the junction (Supplementary Fig. S4C and Fig. 2B).

Compared to the Guanine-I riboswitch, the Guanine-II riboswitch incorporates additional nucleotides in the junction, including A41 in J2/3 and C59–G62 in J3/1, which are highlighted by red circles (Fig. 2A). While C60, located on the exterior of the helix axis, remains isolated and unpaired, most of these extra nucleotides are involved in extensive hydrogen-bonding interaction with other nucleotides within the junction (Fig. 2C and D). Specifically, N1 of A41 forms a hydrogen bond with 4-NH_2 of C59, A61 forms a *trans* Watson–Crick/Hoogsteen base pair with A11 in J1/2, and G62 in J3/1 forms a canonical Watson–Crick base pair with C40 in J2/3 (Fig. 2D). These base pairs A41·C59, A11·A61, and C40·G62 stack consecutively with each other and coaxially extend stem P3 in the tertiary structure (Fig. 2C and Supplementary Fig. S4D). The interplay of these hydrogen-bonding and stacking interactions define the junction structure and stabilize the conformation of the entire riboswitch.

Next, we conducted ITC experiments to validate these intricate interactions within the junction. The U36A and C37A mutants, which disrupt the base triplets of U7-A66·U36 and A8-U65·C37, significantly reduce guanine binding affinity (Supplementary Fig. S4A and B, and Fig. 2E). Similarly, mutations of the nucleotides in J1/2 (U9A, A10U, and A11C) disrupt the hydrogen-bonding interactions of U9-A39, A10·G33, and A11·A61, resulting in a complete loss of guanine binding activity (Fig. 2C and D, and Supplementary Fig. S4C). The A39C mutant exhibits a reduction in guanine binding affinity, suggesting that the stacking interaction of the U9-A39 base pair plays a role in maintaining ligand-binding pocket (Fig. 2E). Additionally, mutations of the extra nucleotides (A41C and G62C) disrupting the involved interactions and continuous base stacking (A41·C59, A11·A61, and C40·G62) also lead to a decrease in guanine binding affinity (Fig. 2E). Together, these results confirm that the stacking interactions of these additional nucleotides play a crucial role in stabilizing the tertiary structure of the PRT riboswitch.

The architecture of binding pocket in PRT Guanine-II riboswitch

As shown in Fig. 3A, the bound guanine (shown in stick representation) is encapsuled within the binding cavity (shown in surface representation), which is formed by three regions of the internal junction and stem P1 (Supplementary Fig. S4E). A base quartet comprising guanine, U34, U38, and C64 is sand-

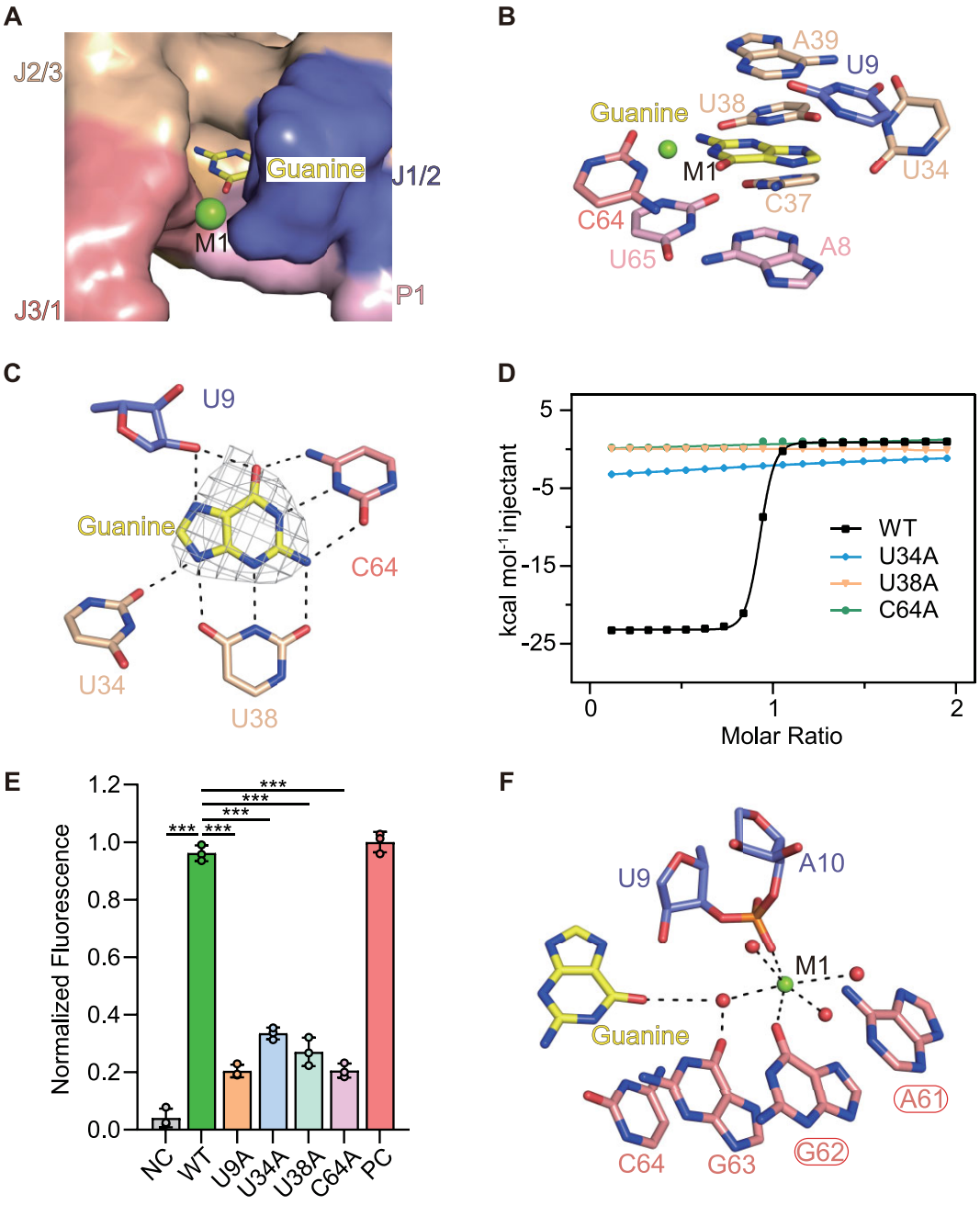

Figure 3. Ligand interactions between guanine and the Guanine-II riboswitch. (**A**) Guanine (shown in stick) is bound in the binding pocket of the Guanine-II riboswitch (shown in surface), which is constituted by the junction regions and stem P1. One metal ion (M1) is positioned within the binding cavity (shown in sphere). (**B**) Guanine pairs with U38 and C64, and is sandwiched by base pair U9-A39 and base triplet A8-U65·C37. (**C**) Guanine forms a canonical Watson–Crick base pair with C64, a noncanonical base pair with U38 via its sugar edge, two hydrogen bonds with 2′-OH of U9 via its sugar edge, and one hydrogen bond with O2 of U34 through its N9. $F_{observed} - F_{calculated}$ ($F_o - F_c$) omit electron-density map contoured at level 3.0 σ of guanine is shown. The map was calculated with the final refined model in which the ligand was removed. (**D**) Overlay of ITC titration heat plot of Guanine-II riboswitch and its mutants (U34A, U38A, and C64A). WT refers to the wildtype PRT riboswitch in Fig. 1A. (**E**) EGFP fluorescence reporter assay of Guanine-II riboswitch and its mutants. All the constructs, NC (negative control) and PC (positive control), are shown in Supplementary Fig. S5. Data are presented as the mean ± SD of three replicates. Background fluorescence was subtracted using the construct lacking EGFP expression and net fluorescence of all construct was normalized with PC. An unpaired *t*-test was employed to assess the significance of differences between WT and NC, as well as among other mutants. Significance was taken at $^{***}P < .001$. (**F**) Interaction between Guanine-II riboswitch and metal ion M1. M1 forms direct coordination with G62 and the phosphate of A10, while it forms indirect coordination with guanine and G63.

wiched between the ceiling formed by the U9-A39 and the floor formed by the A8-U65·C37 base triplet (Supplementary Fig. S4B and Fig. 3B). Within the binding pocket, the Watson–Crick edge of guanine forms a canonical base-pairing interaction with C64, while the sugar edge of guanine engages in non-canonical base-pairing interaction with U38. Additionally, its Hoogsteen edge forms two hydrogen bonds with the 2′-OH of U9, and its N9 forms one hydrogen bond with the O2 of U34 (Fig. 3C).

To assess the importance of these interactions, we generated U34A, U38A, and C64A mutants, which disrupt the hydrogen-bonding interactions with guanine. ITC experiments revealed that these mutations completely abolished guanine binding affinity, highlighting the critical role of these residues in guanine recognition (Fig. 3D and Supplementary Table S2). We further performed reporter assays to evaluate the impact of core base mutations on the gene expression regulation capacity of the PRT riboswitch. As previously reported [18], upon guanine binding, the Guanine-II riboswitch activates the downstream gene expression. To test this, we fused the WT and mutant (U9A, U34A, U38A, and C64A) PRT riboswitch to an EGFP reporter gene (Supplementary Fig. S5A). As a negative control (NC), we designed a construct in which the pairing sequence in the expression platform of the PRT riboswitch was retained, but the guanine binding region was removed. This allowed proper formation of hairpin-dependent terminator with a poly-U tail, therefore preventing EGFP expression (Supplementary Fig. S5B). Correspondingly, we designed a construct as a positive control (PC) in which the downstream transcriptional regulatory sequence was deleted (Supplementary Fig. S5C). Compared to the NC, the WT PRT riboswitch (PRT-WT) increases the expression of EGFP by 23.7 folds and exhibits expression levels comparable to the PC (Fig. 3E). In contrast, mutations in nucleotides directly involved in guanine binding, such as U9A, U34A, U38A, and C64A, reduced EGFP expression to varying degrees (Fig. 3E). All these results are consistent with the ligand-binding pattern of guanine to the PRT riboswitch, as illustrated in the tertiary structure and binding pocket diagram.

As previously reported [18], in the absence of guanine, the Guanine-II riboswitch adopts a stable terminator structure consisting of a hairpin, followed by a poly(U) tail. Upon guanine binding, a stable stem helix is formed, which prevents the formation of the terminator structure, thereby activating downstream gene expression. It can be speculated that when guanine concentrations are sufficient, the downstream genes regulated by the Guanine-II riboswitch become activated. These genes are primarily associated with PRT enzymes involved in the purine salvage pathway, converting guanine into downstream metabolites such as GMP [18]. In contrast, the downstream genes of the Guanine-I riboswitch are mainly associated with XPRTase and are activated only under guanine-deficient conditions, enabling the conversion of alternative purines, such as xanthine, into xanthosine monophosphate (XMP), which can subsequently be converted into GMP [13]. Guanine-I and Guanine-II riboswitches function through distinct mechanisms and sometimes coexist within the same species to maintain the cellular guanine homeostasis.

Within the binding cavity, one Mg^{2+} ion (M1) is identified between J1/2 and J3/1 (Fig. 3A, B, and F). The presence of this Mg^{2+} ion was confirmed by soaking the crystal in the presence of Mn^{2+}, a divalent metal with anomalous scattering properties. The calculated anomalous scattering signal from the diffraction data of the Mn^{2+}-soaked crystal identified the position of the soaked Mn^{2+} (Mn1), which is indicative of the Mg^{2+} (M1) binding site (Fig. 3F and Supplementary Fig. S6). M1 directly interacts with A10 and G62 and establishes an extensive hydrogen bond network through metal-coordinated water molecules (Fig. 3F). ITC experiments demonstrated that in the absence of Mg^{2+}, the PRT riboswitch exhibits no affinity for guanine (Supplementary Fig. S7A and Supplementary Table S2). As the Mg^{2+} concentration increases, the riboswitch's affinity for guanine gradually improves, with dissociation constants of 4.1 μM at 0.5 mM Mg^{2+}, 0.156 μM at 1 mM Mg^{2+}, 0.016 μM at 5 mM Mg^{2+}, and 0.015 μM at 20 mM Mg^{2+} (Supplementary Fig. S7B–E and Supplementary Table S2). Additionally, we assessed the impact of other divalent ions on guanine binding. Compared to Mg^{2+}, guanine binding affinity slightly increased in the presence of Ca^{2+} or Ba^{2+} but decreased by an order of magnitude in the presence of Mn^{2+} (13 nM at 10 mM Ca^{2+}, 5 nM at 10 mM Ba^{2+}, 158 nM at 10 mM Mn^{2+}; Supplementary Fig. S8A–D and Supplementary Table S2). These results indicated that the high-affinity binding of guanine to the Guanine-II riboswitch is strictly dependent on divalent metal ions.

The structure of PRT Guanine-II riboswitch bound to hypoxanthine, guanosine, and 2′-dG

As reported for the Guanine-II riboswitch, the PRT riboswitch binds to certain guanine derivatives [18]. To further characterize its ligand specificity, we measured the binding affinities of guanine analogs (hypoxanthine and xanthine) and N9-modified guanine derivatives (guanosine and 2′-dG) to the PRT riboswitch with ITC titrations (Fig. 4A and B). The PRT riboswitch exhibits similar affinities for guanosine (K_d = 11.0 μM) and 2′-dG (K_d = 8.5 μM), binds to hypoxanthine (K_d = 3.1 μM), but does not recognize xanthine (Supplementary Fig. S9A–D). To elucidate the molecular recognition mechanism of the PRT riboswitch, we determined the crystal structures of its complexes with these guanine derivatives. The X-ray crystallography statistic data of these structures are summarized in Supplementary Table S2. All complex structures adopt a highly similar overall conformation, as shown in the schematic secondary structures and the alignments of the tertiary architectures (Supplementary Fig. S10). The RMSD values for their alignments with the guanine-bound structure are notably low (<1 Å), with 0.721 Å for hypoxanthine, 0.572 Å for guanosine, and 0.466 Å for 2′-dG, highlighting the structural conservation of the binding pocket across different ligands.

As shown in Fig. 4C–H, the binding pockets of these structures were subsequently compared. Alignments of the Guanine-II riboswitch bound to hypoxanthine (in pink) and guanine (in gray) revealed that their binding pocket composition and conformation are highly similar, except for A35, which is positioned outward and adopts a rotated base conformation (Fig. 4C). Notably, hypoxanthine lacks the amino group at the C2 position, forming fewer hydrogen bonds with U38 and C64, therefore resulting in lower binding affinity for hypoxanthine (Fig. 4B–D, Supplementary Fig. S10A, and Supplementary Table S2).

In contrast, significant structural differences in J2/3 region were observed in the binding pockets when comparing the guanosine-bound (in wheat) and 2′-dG-bound (in slate) structures with the guanine-bound complex structure (Fig. 4E and

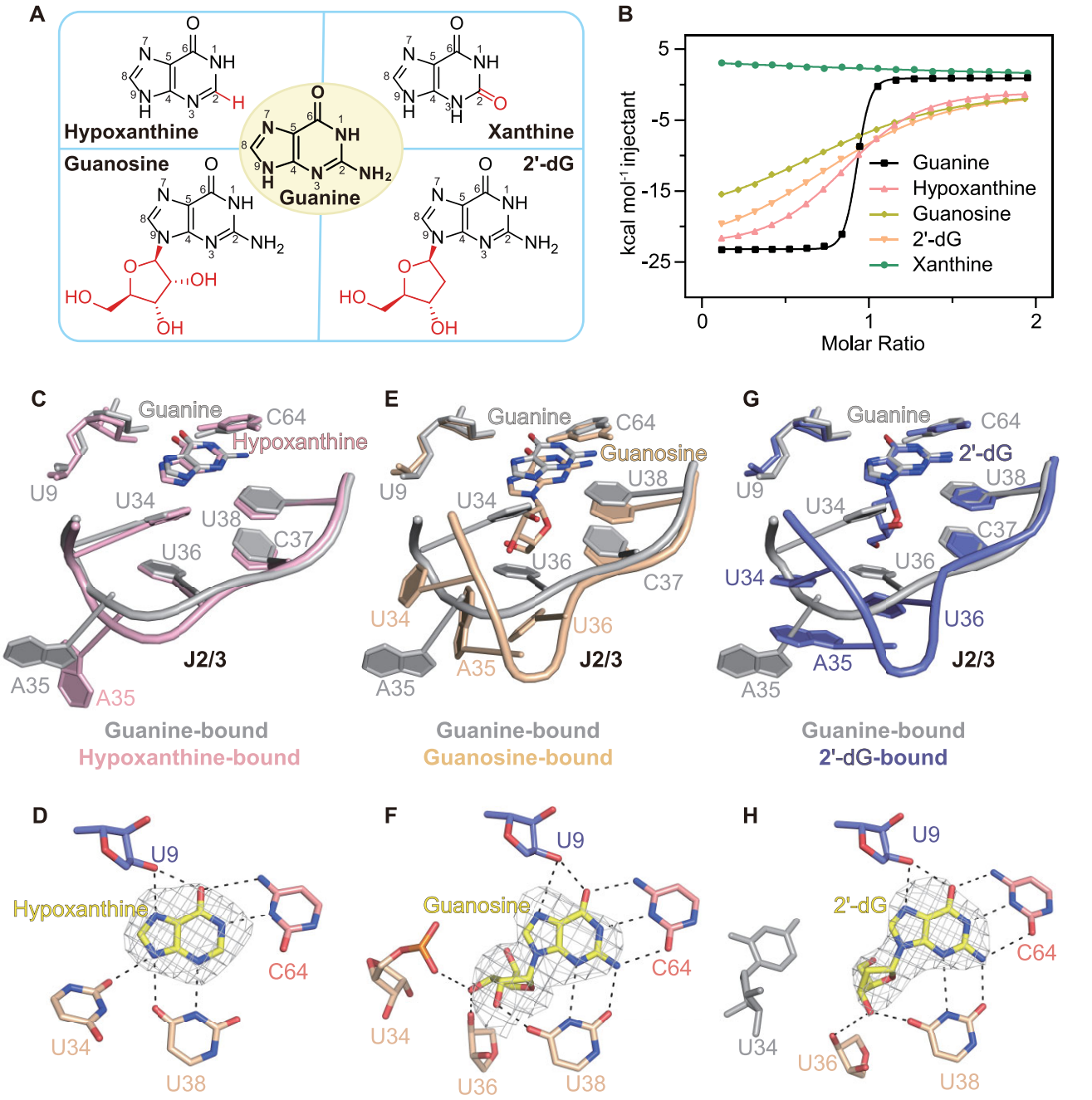

Figure 4. Structure details of PRT Guanine-II riboswitch bound to hypoxanthine, guanosine, and 2′-dG. (**A**) Chemical structure of guanine and its analogs, including hypoxanthine, xanthine, guanosine, and 2′-dG, with variable moiety labeled in red. (**B**) Overlay of ITC titration heat plot comparing the binding of Guanine-II riboswitch to guanine and its analogs. (**C**) Structural alignment of the J2/3 regions of Guanine-II riboswitch bound to guanine (in gray) and hypoxanthine (in pink), showing a RMSD of 0.436 Å. (**D**) Binding pocket interactions of Guanine-II riboswitch bound to hypoxanthine. (**E**) Structural alignment of the J2/3 regions of Guanine-II riboswitch bound to guanine (in gray) and guanosine (in wheat), showing a RMSD of 1.067 Å. (**F**) Binding pocket interactions of Guanine-II riboswitch bound to guanosine. (**G**) Structural alignment of the J2/3 regions of Guanine-II riboswitch bound to guanine (in gray) and 2′-dG (in slate) showing a RMSD of 1.185 Å. (**H**) Binding pocket interactions of Guanine-II riboswitch bound to 2′-dG, with the noninteracting U34 residue shown in gray. $F_{observed} - F_{calculated}$ ($F_o - F_c$) omit electron-density map contoured at level 3.0 σ of all the related compounds are shown. The map was calculated with the final refined model in which the ligand was removed.

G). Both A35 and U36 undergo outward displacement, preventing the formation of the base triplet U7-A66·U36 (Fig. 4E and G, and Supplementary Figs S4A and S10B andC). Additionally, U34 exhibits a notable conformational change, rotating from an inward-facing position relative to the bound ligand to an outward-facing position (Fig. 4E–H). Compared to guanine, guanosine and 2′-dG have ribose or deoxyribose at the N9 position, preventing the formation of hydrogen bonds between N9 and U34, as well as U38 (Figs 3C and 4E–H). Nonetheless, the ribose/deoxyribose of the bound guanosine and 2′-dG form additional hydrogen bonds with the nucleotides in J2/3. In both guanosine-bound and 2′-dG-bound complexes, U34 shifts outward, eliminating its interaction with 2′-dG (Fig. 4H), but forming one hydrogen bond with

O3′ of guanosine via its phosphate oxygen (Fig. 4F). Additionally, U36 interacts with the 3′-OH of the bound guanosine and 2′-dG (Fig. 4F and H). U38 retains two hydrogens bonds to N3 and 2-NH_2 of the bound guanosine and 2′-dG, while forming one hydrogen bond with 2′-OH of the bound guanosine and one hydrogen bond with 3′-OH of the bound 2′-dG through its O4, respectively, replacing the hydrogen bond with N9 observed in guanine binding (Figs 3C and 4F and H).

The Guanine-II riboswitches in complex with different ligands exhibit similar tertiary structures, but variations in the binding pocket conformation and hydrogen-bonding interactions lead to reduced affinity for ligands other than guanine (Supplementary Fig. S10D–F and Fig. 4B–H). Notably, the presence of a ribose or deoxyribose moiety in guanosine and 2′-dG induces significant local conformational changes in J2/3. These structural adjustments expand the binding pocket to accommodate the additional sugar moiety, enabling guanosine and 2′-dG to bind, albeit with lower affinity.

Comparison of the Guanine-II riboswitch with Guanine-I and Xanthine-II riboswitches

Both the Guanine-II and Xanthine-II riboswitches originate from variants of the Guanine-I riboswitch family, sharing similar sequence and secondary structures [18]. The alignments of tertiary structures demonstrate that the Guanine-II riboswitch maintains a conserved overall architecture with both Guanine-I and Xanthine-II riboswitches, with only structural deviations in selected regions (Supplementary Fig. S11). However, these riboswitches exhibit distinct binding specificities [18]. To elucidate the molecular basis of the specificity, we conducted a detailed structural comparison between Guanine-I, Guanine-II, and Xanthine riboswitches (Fig. 5A–C). As shown in Fig. 5A–C, all three riboswitches stabilize their bound ligands through one conserved base quartet formed with nucleotide from the junctions: guanine-U47-U51-C74 in Guanine-I, guanine-U34-U38-C64 in Guanine-II, and xanthine-U33-G37-C64 in Xanthine-II. Additionally, they share two conserved base triplets (A-U·C and U-A·U) below the bound ligand, and feature a purine nucleotide (A73 in Guanine-I, G63 in Guanine-II, and G63 in Xanthine-II) along with a conserved U-A base pair (U22-A52 in Guanine-I, U9-A39 in Guanine-II, and U8-A38 in Xanthine-II) above the bound ligand (Fig. 5A–C).

However, the presence of additional bases (indicated by red dashed line) in the Guanine-II and the Xanthine-II riboswitches introduces further structural differences (Fig. 5B and C). In Guanine-II riboswitch, C40 in J2/3 pairs with G62 in J3/1, whereas in Guanine-I, the corresponding nucleotide C53 rotates to the opposite side and pairs with G46 within J2/3 (Fig. 5E and F). Interestingly, in Xanthine-II riboswitch, C40 in J2/3 also pairs with G62 in J3/1, similar to Guanine-II, while the inserted nucleotide C39 shifts to G32 and pairs within J2/3, resembling Guanine-I (Fig. 5E–G). Consequently, in Guanine-I and Xanthine-II, a base triplet A·G-C (A23·G46-C53 in Guanine-I and A9·G32-C39 in Xanthine-II) is formed above the U-A base pair (U22-A52 in Guanine-I and U8-A38 in Xanthine-II) (Fig. 5A, C, E, and G). In contrast, in Guanine-II, distinct paring interactions between A10·G33 and C40-G62 are formed above U9-A39 (Fig. 5B and F). Additionally, in Xanthine-II, the base pair C40-G62 is also formed (Fig. 5C and G). Above C40-G62, both Guanine-II and Xanthine-II adopt similar conformation supporting stem P3, in which two adenines (A11 and A41 in Guanine-II, A10 and A41 in Xanthine-II) form two stacked noncanonical base pairs with A61 and C59 in J3/1, respectively (Fig. 5B, C, F, and G). Compared to Guanine-II and Xanthine-II, Guanine-I contains fewer nucleotides in the junction and adopts a more compact conformation (Fig. 5A and E). The corresponding nucleotide A24 does not participate in pairing interactions but directly stacks between A73 and the terminal of stem P3 (Fig. 5E).

As reported [17, 24] and confirmed by our ITC titration, the Guanine-I riboswitch binds guanine and various guanine derivatives, including hypoxanthine, xanthine, guanosine, and 2′-dG (Fig. 5D, Supplementary Fig. S9E, and Supplementary Table S2). Compared to the Guanine-I riboswitch, the Guanine-II riboswitch exhibits comparable affinities for guanine, guanosine, and 2′-dG but significantly reduced affinity for hypoxanthine. Moreover, the Guanine-II riboswitch shows no detectable binding to xanthine under varying pH conditions (Fig. 5D and Supplementary Fig. S9D), indicating higher ligand-binding specificity. Compared to Guanine-I and Guanine-II riboswitches, the Xanthine-II riboswitch demonstrates more specific binding activity to xanthine, despite having a relatively lower binding affinity for its native ligand (Fig. 5D) [26].

Previous research has revealed that mutations in the binding pocket of Guanine-I riboswitch can alter ligand specificity [27–29]. As shown in Supplementary Fig. S12A, the C74U mutant shifts the ligand preference of Guanine-I from guanine to adenine [27], while the U51C mutant drastically reduces the affinity for guanine ($K_d = 42$ μM) but retains strong binding to 2′-dG ($K_d = 9$ μM), enabling specific recognition of 2′-dG [28, 29]. The structural alignment shows that the binding pocket of the Guanine-II riboswitch closely resembles that of the Guanine-I riboswitch, with an additional hydrogen bond present in Guanine-II (Fig. 5H). To investigate whether similar mutations affect ligand specificity in Guanine-II riboswitches, we performed ITC experiments on the corresponding nucleotide mutant (C64U and U38C) of the PRT riboswitch (Supplementary Fig. S12B). The WT PRT riboswitch binds guanine but not adenine, whereas the corresponding nucleotide mutant C64U fails to bind either ligand (Supplementary Fig. S12C–E). Meanwhile, the corresponding nucleotide mutant U38C exhibits reduced binding affinity for guanine ($K_d = 1.3$ μM) and no binding activity to 2′-dG, yet still retains specific recognition for guanine, differing from the ligand specificity of Guanine-I U51C mutant (Supplementary Fig. S12F and G). Although the WT and mutants of Guanine-I and Guanine-II share the same ligand-binding pocket and similar overall structure, differences in the local conformation of the junction lead to distinct specificity for guanine, adenine, or 2′-dG (Fig. 5H and Supplementary Figs S11A and S12A and B). These comparisons highlight that even when the binding pocket composition of two riboswitches is conserved, variations in surrounding bases alone can significantly alter ligand specificity.

Comparing the sequences of Guanine-II and Xanthine-II riboswitches reveals two key differences in their junctions, where U38 in Guanine-II is replaced by G37 in Xanthine-II, and an additional base, C39, is inserted into Xanthine-II (Supplementary Fig. S13A and B). In Xanthine-II, C39 is involved in the formation of the A9-G32·C39 base triplet, whereas in Guanine-II, only the base pair A10·G33 is present (Supplementary Fig. S13C). Additionally, structural alignment of their binding pockets shows that U38 in Guanine-II and

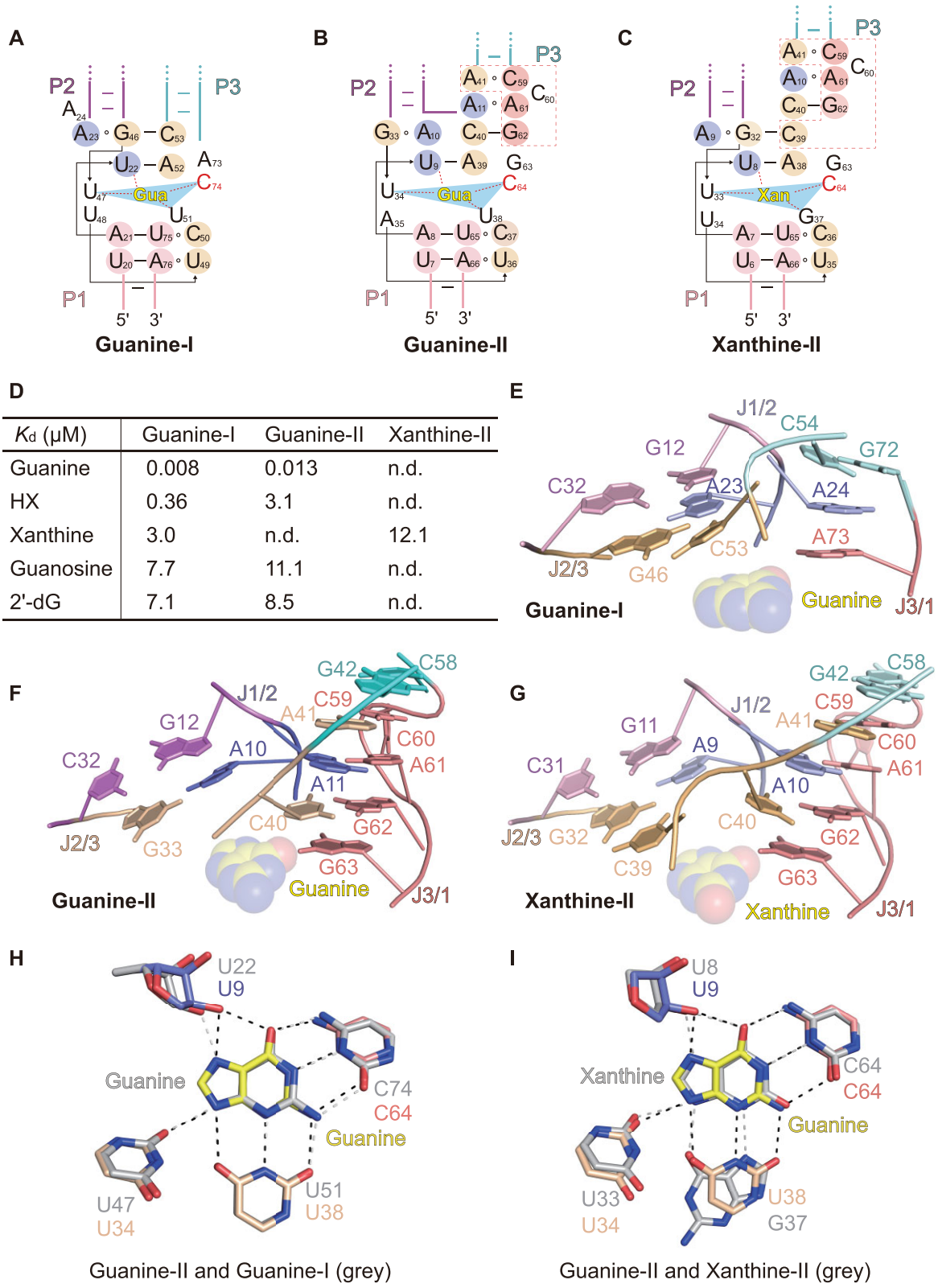

K_d (μM)	Guanine-I	Guanine-II	Xanthine-II
Guanine	0.008	0.013	n.d.
HX	0.36	3.1	n.d.
Xanthine	3.0	n.d.	12.1
Guanosine	7.7	11.1	n.d.
2'-dG	7.1	8.5	n.d.

Figure 5. Comparison between the Guanine-I, Guanine-II, and Xanthine-II riboswitches. Schematic representations of the Guanine-I (**A**), Guanine-II (**B**), and Xanthine-II (**C**) riboswitches. The nucleotides involved in different interaction layers within core regions are color-coded to the cartoon representation. The unique nucleotides distinguishing the Guanine-II and Xanthine-II riboswitches from the Guanine-I riboswitch are highlighted with red dashed lines. (**D**) Comparison of ITC titration binding affinity between Guanine-I, Guanine-II, and Xanthine-II riboswitches binding to guanine and its analogs, with n.d. referring to no binding. An expanded view of the junction composition of Guanine-I (**E**), Guanine-II (**F**), and Xanthine-II (**G**) riboswitches. Ligands are shown in sphere. (**H**) Structural alignment of the binding pockets of the Guanine-II and Guanine-I (in gray) riboswitches, showing an RMSD of 0.382 Å. (**I**) Structural alignment of the binding pockets of the Guanine-II and Xanthine-II (in gray) riboswitches, showing an RMSD of 0.483 Å.

G37 in Xanthine-II form specific interactions with their respective ligands guanine and xanthine (Fig. 5I). This suggests that despite their similar tertiary structures, differences in the key binding pocket bases dictate distinct ligand recognition patterns. To validate this, we performed ITC experiments on U38G, I39C (insertion of a nucleotide C between A39 and C40), and U38G-I39C mutants of the PRT riboswitch (Supplementary Fig. S13A). The results showed that U38G mutant does not bind to either guanine or xanthine (Supplementary Fig. S13D and E). In contrast, I39C mutant binds to guanine with K_d of 0.0017 μM and xanthine with K_d of 9.79 μM (Supplementary Fig. S13F and G), consistent with the recognition properties of the Guanine-I riboswitch (K_d = 0.008 μM for guanine and K_d = 3.0 μM for xanthine; Fig. 5D). The inserted nucleotide C likely forms a A·G-C base triplet, which exists in both Guanine-I and Xanthine-II (Fig. 5A and C, and Supplementary Fig. S13C), and determines xanthine recognition. Furthermore, U38G-I39C mutant binds to xanthine (K_d = 14.6 μM) but not to guanine (Supplementary Fig. S13H and I), mirroring the binding behavior of the Xanthine-II riboswitch (K_d = 12.1 μM for xanthine and no binding affinity for guanine; Fig. 5D) [26]. These findings indicate that the ligand recognition specificity switch from guanine to xanthine in the Guanine-II riboswitch is mainly determined by both the U38G mutation in the binding pocket and the insertion of nucleotide C in the peripheral structure. Besides, it can be speculated that the U51G mutant of Guanine-I may result in specific xanthine binding and a loss of guanine recognition.

Structure-based rational search for additional compounds binding to Guanine-II riboswitch

The recognition mechanism of the Guanine-II riboswitch for guanine is reminiscent of that of the THF-II riboswitch, which, while structurally distinct from the Guanine-II riboswitch (Fig. 1C and D, and Supplementary Fig. S14), is capable of binding guanine, guanine derivatives, and pterin derivatives [30]. Structural alignments of the ligand-binding pockets between Guanine-II and THF-II (PDB: 8XZW) riboswitches, both bound to guanine (Supplementary Fig. S14C), indicate that the bases of C18 and U41 in THF-II align with U38 and C64 in Guanine-II, forming equivalent hydrogen bonds with their respective ligands. Given the observed ability of the Guanine-II riboswitch binding pocket to accommodate either ribose or deoxyribose (Fig. 4F and G), along with the similarity of the binding pockets between Guanine-II and THF-II riboswitches, we speculated that the Guanine-II riboswitch could also bind to THF. This was subsequently confirmed by ITC experiments, which revealed that the Guanine-II riboswitch binds to THF with a K_d of 3.76 μM (Supplementary Fig. S15A), suggesting that the Guanine-II riboswitch has potential to interact with other structurally related compounds.

To identify the possible ligands for the Guanine-II riboswitch, we first screened C8-modified guanine analogs, including 8-methylguanine, 8-aminoguanine, 8-oxoguanine, and 8-azaguanine (Fig. 6A). ITC experiments were conducted to assess their binding affinity to the PRT riboswitch, yielding the dissociation constants of K_d = 44.0 μM for 8- methylguanine, K_d = 11.2 μM for 8-aminoguanine, K_d = 0.65 μM for 8-oxoguanine, and K_d = 1.81 μM for 8-azaguanine (Supplementary Fig. S15B–E and Supplementary Table S2). Compared to the Guanine-I riboswitch, which binds guanine derivatives such as 8-oxoguanine (K_d = 10 nM) and 8-aminoguanine (K_d = 36 nM) with markedly high affinity[31], the Guanine-II riboswitch exhibits significantly lower binding affinity for these compounds, highlighting its enhanced specificity for guanine. To elucidate the structural basis for this binding discrimination, we solved the crystal structures of the PRT riboswitch in complex with each of these ligands (Supplementary Table S1). Compared to the guanine-bound structure, the presence of the 8-methyl group in 8-methylguanine causes steric hindrance between U34 and the N9 position, which likely disrupts optimal hydrogen bonding and accounts for the reduced binding affinity observed in ITC experiments (Supplementary Fig. S15B and Fig. 6B). Although 8-NH_2 of 8-aminoguanine forms hydrogen bonds with U34 and A8, and the 8-oxo group of 8-oxoguanine interacts with A8 (Fig. 6C–D), both ligands exhibit only a single hydrogen bond with U9 due to the increased distance, contributing to their lower affinities relative to guanine (Supplementary Fig. S15C and D). While 8-azaguanine forms interactions similar to those of guanine, its potential for tautomeric interconversion may weaken hydrogen-bonding networks, thereby reducing its affinity for the Guanine-II riboswitch (Supplementary Fig. S15E and Fig. 6E). Overall, these findings demonstrate that the Guanine-II riboswitch maintains micromolar affinity for various C8-modified guanine analogs, underscoring its capacity to accommodate chemical modifications, while preserving a degree of ligand selectivity.

The second group of compounds we tested are pterin and its derivatives, including isoxanthopterin, tetrahydrobiopterin (BH_4), and DHN (Fig. 6A). These compounds exhibit similar structural interfaces to guanine derivatives, that could potentially interact with the Guanine-II riboswitch. ITC experiments revealed that the PRT riboswitch exhibits a binding affinity of K_d = 2.68 μM for isoxanthopterin, K_d = 6.42 μM for BH_4, and K_d = 6.27 μM for DHN, but does not bind to pterin (Supplementary Fig. S15F–I and Supplementary Table S2). To explore the molecular mechanism for binding of pterin and its derivatives, we further solved the crystal structures of the PRT riboswitch in complex with these three ligands (Supplementary Table S1). Structural comparison indicated that isoxanthopterin, BH_4, and DHN form base-pairing interactions with both U38 and C64, similar to the guanine-bound structure, thereby stabilizing ligand binding (Supplementary Fig. S15G–I and Fig. 6A and F). Here, it is noted that N8 of pterin is unable to form a hydrogen bond with U38, which may account for the loss of binding affinity to the Guanine-II riboswitch (Supplementary Fig. S15F and Fig. 6A). Compared to the guanine-bound structure, both BH_4 and DHN show no interaction with U34, instead, the C6 attached groups of BH_4 and DHN form hydrogen bonds with A8 and U9, further stabilizing the binding (Fig. 6A, G, and H). These findings suggest that compounds with similar structures may follow a common ligand recognition pattern, interacting with RNAs of diverse folds. Furthermore, these compounds expand the chemical space for riboswitch-targeted drug development. The structural insights provided here offer a framework for rational drug design by elucidating key ligand-binding interactions.

Conclusion

The presence of additional inserted bases in the junctional region endows the Guanine-II riboswitch with a distinct ligand-

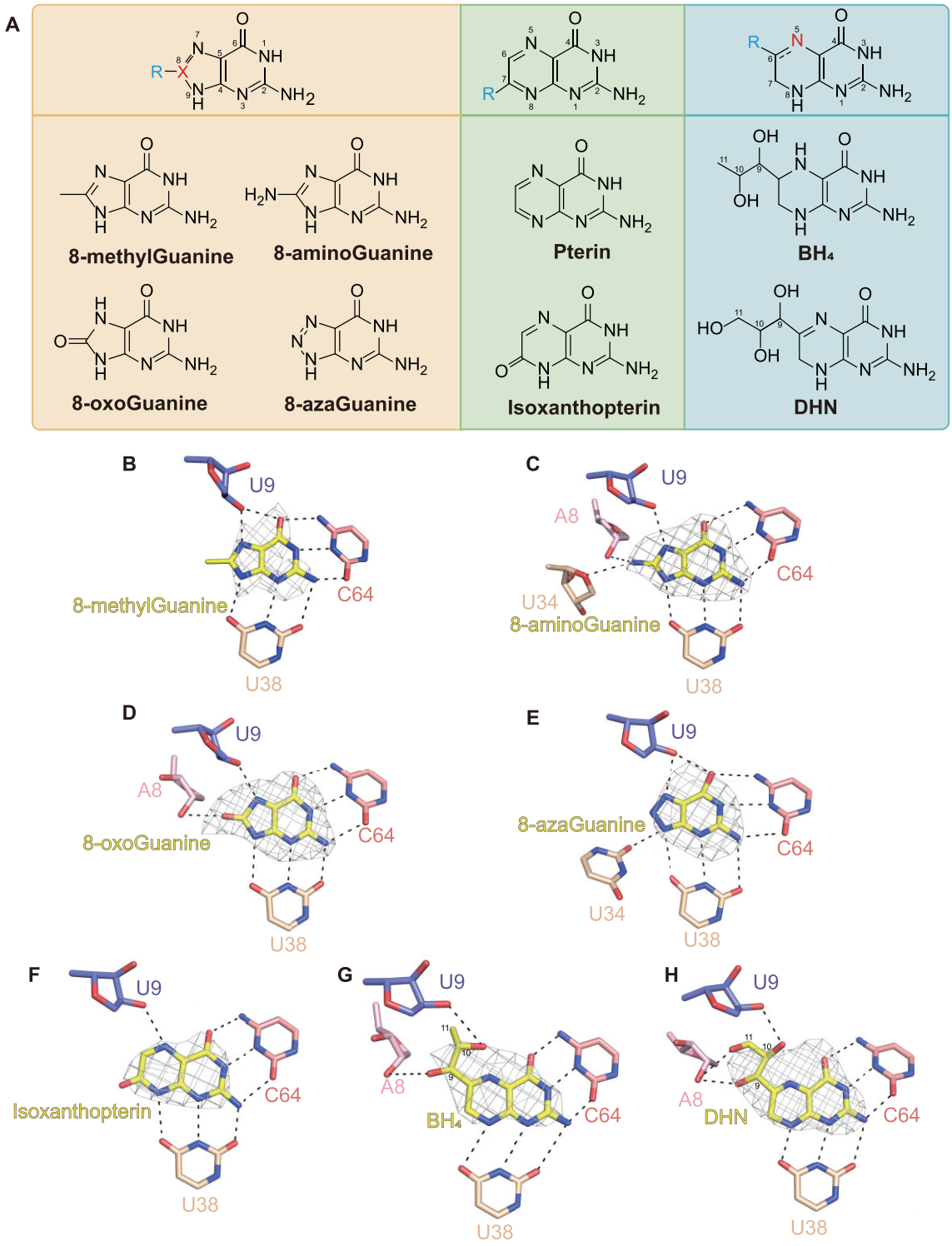

Figure 6. Structure-based rational search for the bound compound of Guanine-II riboswitch. (**A**) Chemical structure of C8-modified guanine derivatives, pterin, and its derivatives. Binding pocket interactions of Guanine-II riboswitch bound to C8-modified guanine derivatives, including 8-methylguanine (**B**), 8-aminoguanine (**C**), 8-oxoguanine (**D**), and 8-azaguanine (**E**). Binding pocket interactions of Guanine-II riboswitch bound to pterin derivatives, including isoxanthopterin (**F**), BH_4 (**G**), and 7,8-dihydroneopterin (DHN) (**H**). $F_{observed} - F_{calculated}$ ($F_o - F_c$) omit electron-density map contoured at level 3.0 σ of all the related compounds are shown. The map was calculated with the final refined model in which the ligand was removed.

recognition specificity distinct from that of the Guanine-I riboswitch [18]. We determined the PRT Guanine-II riboswitches in complex with guanine, hypoxanthine, guanosine, and 2′-dG (Figs 1 and 4). Structural comparison revealed that nucleotide variations in the junctional regions influence ligand-binding selectivity and specificity. The additional nucleotides in J3/1 extensively interact with those in J1/2 and J2/3, tightening the J1/2 and J2/3 junctions in the tertiary structure and forming a platform to support stem P3 (Fig. 2). These interactions play a crucial role in maintaining structural stability. Structural analysis of the J2/3 region in guanosine and deoxyguanosine complexes revealed structural folding flexibility in U34-A35-U36, allowing accommodation of both ribose and deoxyribose moieties, thereby enabling tolerance for sugar modifications in ligands (Fig. 4C–H). However, the conserved nucleotides C64 and U38 adopt a consistent conformation across these structures, ensuring high specificity for the guanine moiety (Fig. 4E–H). This results in decreased binding affinity for hypoxanthine and complete loss of xanthine recognition in the Guanine-II riboswitch (Fig. 4C and D). The impact of these bases' variation in the junctional region of guanine family riboswitch may aid in identification of riboswitches with enhanced specificity for guanine derivatives.

Through comprehensive structural comparisons of different variants of the guanine riboswitch family including Guanine-II, Guanine-I, and Xanthine-II riboswitches, we identified significant structural variations that contribute to their distinct ligand specificities. While Guanine-II and Guanine-I riboswitches adopt a conserved overall tertiary architecture and an identical ligand-binding pocket, local structural differences surrounding the binding pockets confer distinct ligand recognition specificities (Supplementary Fig. S11A and Fig. 5H). Notably, variations in the junction regions result in different interaction layers, and the J3/1 region adopts a W-shaped structure—comprising three closely consecutive bends formed by nucleotides C58 to C64—which markedly differs from its counterpart in the Guanine-I riboswitch and contributes to the enhanced specificity for guanine (Fig. 5A, B, E, and F, and Supplementary Fig. S11A). ITC experiments on the mutants further confirmed these specificity difference for guanine, adenine, and 2′-dG (Supplementary Fig. S12). In contrast, Guanine-II and Xanthine-II riboswitches exhibit similar overall structures but possess distinct ligand-binding pockets (Supplementary Fig. S11B and Fig. 5I), resulting in different ligand-recognition profiles. Our experimental validation demonstrated that the Guanine-II riboswitch specifically recognizes guanine through U38, while the U38G-I39C mutation switches its specificity to xanthine (Supplementary Fig. S13). This two-nucleotide switching mechanism, analogous to the transition between the Guanine-I and Adenine riboswitches, has profound implications for bacterial gene regulation [16, 27, 28].

Although the Guanine-II and THF-II riboswitches adopt distinct tertiary folds, they utilize similar recognition patterns to interact with their native ligands within the binding pockets (Figs 1 and 3, and Supplementary Fig. S14). This similarity highlights both the structural diversity of RNA and the conservation of small-molecule recognition mechanisms. Structure comparison of their binding pockets prompted the search for additional potential ligands capable of interacting with the Guanine-II riboswitch. Our research identified two distinct classes of compounds that bind to Guanine-II riboswitch and investigated their binding mechanisms through crystal structures of the Guanine-II riboswitch bound with each compound: (i) guanine derivatives, including 8-methylguanine, 8-aminoguanine, 8-oxoguanine, and 8-azaguanine and (ii) pterin derivatives, including isoxanthopterin, BH_4, and DHN (Fig. 6 and Supplementary Fig. S15). These findings significantly expand the known repertoire of small molecules capable of binding to the Guanine-II riboswitch, suggesting that other purine riboswitch variants may likewise accommodate a diverse range of purine and pteridine derivatives. This structural plasticity not only highlights the adaptability of riboswitches to various ligands but also underscores their therapeutic potential. Given the exclusive presence of these riboswitches in numerous pathogenic bacteria and their absence in humans, the identified ligand–riboswitch interactions provide a robust structural foundation for the rational design of novel antimicrobial drugs [31].

Acknowledgements

We thank the staff members of the Large-scale Protein Preparation System, BL-17B, BL-17U1, BL18U1, BL-19U1, and BL02U1 beamlines at the National Facility for Protein Science in Shanghai (NFPS), and Zhangjiang Lab, China for providing technical support and assistance in data collection and analysis. We thank the staff of the BL02U1 beamline at the National Center for Protein Sciences Shanghai (NCPSS) at SSRF for their assistance in X-ray data collection. We thank the technical assistance from the core facility of the Life Sciences Institute (LSI), Zhejiang University.

Author contributions: Hongcheng Li (Investigation [equal])

Supplementary data

Supplementary data is available at NAR online.

Conflict of interest

None declared.

Funding

This work was supported by the National Key Research and Development Program of China [2023YFC2604300 to A.R.], the National Natural Science Foundation of China [32325029, 91940302, and 91640104 to A.R.], the Major Program of Zhejiang Provincial Natural Science Foundation [LD25C050002 to A.R.]. Funding to pay the Open Access publication charges for this article was provided by Zhejiang University.

Data availability

Atomic coordinates and structure factors for the reported crystal structures of the PRT Guanine-II riboswitch in complex with guanine and other analogs have been deposited with the Protein Data Bank (www.rcsb.org) under accession numbers 9LMC (PRT-guanine Mn^{2+} soaking structure), 9LJN (PRT-guanine structure), 9LKE (PRT-hypoxanthine structure), 9LKF (PRT-guanosine structure), 9LKC (PRT-2′-dG structure), 9V50 (PRT-8-methylguanine structure), 9V4Y (PRT-8-aminoguanine structure), 9V4Z (PRT-8-oxoguanine structure), 9V4X (PRT-8-azaguanine structure), 9V4V (PRT-isoxanthopterin structure), 9V4U (PRT-DHN structure), and

9V51 (PRT-BH_4 structure). All study data are included in the article and supplementary materials.

References

1. Mironov AS, Gusarov I, Rafikov R *et al.* Sensing small molecules by nascent RNA: a mechanism to control transcription in bacteria. *Cell* 2002;**111**:747–56. https://doi.org/10.1016/S0092-8674(02)01134-0
2. Winkler WC, Cohen-Chalamish S, Breaker RR. An mRNA structure that controls gene expression by binding FMN.*Proc Natl Acad Sci USA* 2002;**99**:15908–13.
3. Nahvi A, Sudarsan N, Ebert MS *et al.* Genetic control by a metabolite binding mRNA. *Chem Biol* 2002;**9**:1043.
4. Winkler W, Nahvi A, Breaker RR. Thiamine derivatives bind messenger RNAs directly to regulate bacterial gene expression. *Nature* 2002;**419**:952–6. https://doi.org/10.1038/nature01145
5. Serganov A, Nudler E. A decade of riboswitches. *Cell* 2013;**152**:17–24. https://doi.org/10.1016/j.cell.2012.12.024
6. Kavita K, Breaker RR. Discovering riboswitches: the past and the future. *Trends Biochem Sci* 2023;**48**:119–41. https://doi.org/10.1016/j.tibs.2022.08.009
7. Hamal Dhakal S, Kavita K, Panchapakesan SSS *et al.* 8-Oxoguanine riboswitches in bacteria detect and respond to oxidative DNA damage. *Proc Natl Acad Sci USA* 2023;**120**:e2307854120. https://doi.org/10.1073/pnas.2307854120
8. Salvail H, Balaji A, Roth A *et al.* A spermidine riboswitch class in bacteria exploits a close variant of an aptamer for the enzyme cofactor S-adenosylmethionine. *Cell Rep* 2023;**42**:113571. https://doi.org/10.1016/j.celrep.2023.113571
9. Gupta A, Swati D. Riboswitches in Archaea. *Comb Chem High Throughput Screen* 2019;**22**:135–49.
10. Kim JN, Breaker RR. Purine sensing by riboswitches. *Biol Cell* 2008;**100**:1–11.
11. Lane AN, Fan TW. Regulation of mammalian nucleotide metabolism and biosynthesis. *Nucleic Acids Res* 2015;**43**:2466–85. https://doi.org/10.1093/nar/gkv047
12. Pedley AM, Benkovic SJ. A new view into the regulation of purine metabolism: the purinosome. *Trends Biochem Sci* 2017;**42**:141–54. https://doi.org/10.1016/j.tibs.2016.09.009
13. Mandal M, Boese B, Barrick JE *et al.* Riboswitches control fundamental biochemical pathways in *Bacillus subtilis* and other bacteria. *Cell* 2003;**113**:577–86. https://doi.org/10.1016/S0092-8674(03)00391-X
14. Kim JN, Roth A, Breaker RR. Guanine riboswitch variants from *Mesoplasma florum* selectively recognize 2'-deoxyguanosine. *Proc Natl Acad Sci USA* 2007;**104**:16092–7. https://doi.org/10.1073/pnas.0705884104
15. Batey RT, Gilbert SD, Montange RK. Structure of a natural guanine-responsive riboswitch complexed with the metabolite hypoxanthine. *Nature* 2004;**432**:411–5. https://doi.org/10.1038/nature03037
16. Serganov A, Yuan YR, Pikovskaya O *et al.* Structural basis for discriminative regulation of gene expression by adenine- and guanine-sensing mRNAs. *Chem Biol* 2004;**11**:1729–41.
17. Gilbert SD, Reyes FE, Edwards AL *et al.* Adaptive ligand binding by the purine riboswitch in the recognition of guanine and adenine analogs. *Structure* 2009;**17**:857–68. https://doi.org/10.1016/j.str.2009.04.009
18. Hamal Dhakal S, Panchapakesan SSS, Slattery P *et al.* Variants of the guanine riboswitch class exhibit altered ligand specificities for xanthine, guanine, or 2'-deoxyguanosine. *Proc Natl Acad Sci USA* 2022;**119**:e2120246119.
19. Pikovskaya O, Serganov AA, Polonskaia A *et al.* Preparation and crystallization of riboswitch–ligand complexes. *Methods Mol Biol* 2009;**540**:115–28.
20. Adams PD, Afonine PV, Bunkóczi G *et al.* PHENIX: a comprehensive Python-based system for macromolecular structure solution. *Acta Crystallogr D Biol Crystallogr* 2010;**66**:213–21. https://doi.org/10.1107/S0907444909052925
21. Emsley P, Cowtan K. Coot: model-building tools for molecular graphics. *Acta Crystallogr D Biol Crystallogr* 2004;**60**:2126–32. https://doi.org/10.1107/S0907444904019158
22. Murshudov GN, Vagin AA, Dodson EJ. Refinement of macromolecular structures by the maximum-likelihood method. *Acta Crystallogr D Biol Crystallogr* 1997;**53**:240–55. https://doi.org/10.1107/S0907444996012255
23. Weinberg Z, Nelson JW, Lünse CE *et al.* Bioinformatic analysis of riboswitch structures uncovers variant classes with altered ligand specificity. *Proc Natl Acad Sci USA* 2017;**114**:E2077–85. https://doi.org/10.1073/pnas.1619581114
24. Matyjasik MM, Hall SD, Batey RT. High affinity binding of N2-modified guanine derivatives significantly disrupts the ligand binding pocket of the guanine riboswitch. *Molecules* 2020;**25**:2295. https://doi.org/10.3390/molecules25102295
25. Read RJ, Adams PD, Arendall WB *et al.* A new generation of crystallographic validation tools for the Protein Data Bank. *Structure* 2011;**19**:1395–412. https://doi.org/10.1016/j.str.2011.08.006
26. Xu X, He M, Tai X *et al.* Structure-based principles underlying ligand recognition of xanthine-II riboswitch. *Sci China Life Sci* 2025;**68**:2073–84. https://doi.org/10.1007/s11427-024-2800-0
27. Mandal M, Breaker RR. Adenine riboswitches and gene activation by disruption of a transcription terminator. *Nat Struct Mol Biol* 2004;**11**:29–35.
28. Gilbert SD, Stoddard CD, Wise SJ *et al.* Thermodynamic and kinetic characterization of ligand binding to the purine riboswitch aptamer domain. *J Mol Biol* 2006;**359**:754–68. https://doi.org/10.1016/j.jmb.2006.04.003
29. Edwards AL, Batey RT. A structural basis for the recognition of 2'-deoxyguanosine by the purine riboswitch. *J Mol Biol* 2009;**385**:938–48. https://doi.org/10.1016/j.jmb.2008.10.074
30. Li C, Xu X, Geng Z *et al.* Structure-based characterization and compound identification of the wild-type THF class-II riboswitch. *Nucleic Acids Res* 2024;**52**:8454–65. https://doi.org/10.1093/nar/gkae377
31. Panchal V, Brenk R. Riboswitches as drug targets for antibiotics. *Antibiotics* 2021;**10**:45. https://doi.org/10.3390/antibiotics10010045

Received: June 6, 2025. **Revised:** August 13, 2025. **Editorial Decision:** August 15, 2025. **Accepted:** August 21, 2025